Regular and chaotic quantum dynamics in the driven square well

Todd Timberlake
*Department of Physics, Astronomy, and Geology, Berry College, Mount Berry, GA 30149-5004**
(Dated: October 15, 2004)

The quantum dynamics of the periodically-driven infinite square well is examined. This simple system illustrates some important aspects of quantum chaos. The phase space structure of the quantum eigenstates are shown to mimic the structure of the classical phase space and these eigenstates show a transition from "regular" to "chaotic" as the strength of the driving field is increased. The spacing of eigenvalues undergoes a transition from Poisson to COE statistics as the classical system becomes chaotic. High-harmonic generation in the radiation spectrum is shown to be closely tied to the onset of chaos in the classical system.

I. INTRODUCTION

It is now widely recognized that there are two distinct types of motion possible in classical Hamiltonian systems: *regular* motion and *chaotic* motion. Chaotic motion is usually distinguished by its sensitive dependence on initial conditions. The distance between two chaotic trajectories that start off near each other in phase space will increase exponentially in time, while regular trajectories exhibit only polynomial divergence.

Such a distinction between regular and chaotic motion cannot exist in quantum mechanics. The Heisenberg uncertainty principle prevents a particle from simultaneously having well-defined position and momentum, therefore it is impossible to specify a particle's location in phase space. There are no trajectories in quantum mechanics, so the classical criterion for distinguishing regular motion from chaotic motion cannot apply. The question then arises: Can the dynamics of a quantum system whose classical limit ($\hbar \to 0$) is chaotic be distinguished from the dynamics of a quantum system whose classical limit is regular? Studies carried out over the last thirty years show that the answer to this question is yes.

One feature that can be used to distinguish between regular and chaotic quantum systems is the statistical distribution of energy eigenvalues. The eigenvalues of regular systems are randomly distributed, while the eigenvalues of chaotic systems have the same statistical properties as the eigenvalues of random matrices. The eigenvectors of regular systems also differ noticeably from those of chaotic systems. Indeed, the study of the distinctions between regular and chaotic quantum dynamics has matured to the point that there are now several textbooks available on the subject.[1–4]

Understanding the quantum dynamics of classically chaotic systems (or "quantum chaos") has provided a great deal of insight into a number of experimentally observed phenomena, such as high-harmonic generation[5] and multi-photon ionization.[6] More recently, experiments have been conducted to observe specific characteristics of quantum chaos, such as dynamical localization and chaos-assisted tunneling.[7] These experiments, along with many others, have served as both illustrations and tests of the ideas of quantum chaos.

In this paper we examine the classical and quantum dynamics of the periodically driven infinite square well. In the classical version of this system the low-energy trajectories exhibit a transition from regular motion to chaotic motion as the strength of the driving field is increased. The goal of this paper is to illustrate how the quantum eigenvalues and eigenvectors of this system change as the driving field is increased and to connect these changes with the transition to chaos in the classical system.

II. CLASSICAL DYNAMICS

The Hamiltonian for the periodically driven infinite square well system is

$$\tilde{H} = \frac{\tilde{p}^2}{2m} + \tilde{\epsilon}\tilde{x}\cos(\tilde{\omega}_0\tilde{t}),\ |\tilde{x}| \le a, \tag{1}$$

where m is the mass, $\tilde{p}$ is the momentum, and $\tilde{x}$ is the position of the particle. The width of the square well is $2a$. The driving field has amplitude $\tilde{\epsilon}$ and frequency $\tilde{\omega}_0$, with $\tilde{t}$ as the time coordinate. This Hamiltonian can be made dimensionless by the following scaling transformations[8]: $\tilde{H} = Hc$, $\tilde{x} = xa$, $\tilde{p} = p\sqrt{2mc}$, $\tilde{\epsilon} = \epsilon c/a$, $\tilde{t} = ta\sqrt{2m/c}$, and $\tilde{\omega}_0 = (\omega_0/a)\sqrt{c/(2m)}$, where c is a new unit of energy for the scaled system. The new Hamiltonian (in units of c) is

$$H = p^2 + \epsilon x\cos(\omega_0 t),\ |x| \le 1, \tag{2}$$

where all quantities are now dimensionless. There is only one independent parameter in this system since the transformation $(\omega_0, \epsilon) \to (\omega_0\sqrt{c}, \epsilon c)$ is equivalent to a change of the energy unit c. Therefore we can obtain a complete picture of the classical dynamics by choosing an arbitrary value for ω_0 ($\omega_0 = 80$ in this paper) and investigating the dynamics as ϵ is varied.

Let us take a moment to examine the symmetries of this system. The most obvious symmetry is that the Hamiltonian is unchanged by the transformation $p \to -p$, indicating that the dynamics must be symmetric about the axis $p = 0$. The Hamiltonian also is symmetric under the discrete time translation $t \to t + T$, where $T = 2\pi/\omega_0$ is the period of the driving field. Note

that the Hamiltonian is not symmetric under infinitesimal time translations, so energy is not a conserved quantity in this system because the Hamiltonian depends explicitly on time. In addition, this Hamiltonian is symmetric under a generalized parity transformation defined by $x \to -x,\ t \to t + T/2$. For $\epsilon = 0$, of course, the Hamiltonian is symmetric under the more conventional parity transformation $x \to -x$.

For $\epsilon = 0$ the dynamics of this system is extremely simple: the particle bounces back and forth between the walls of the well, maintaining a constant magnitude of momentum. As ϵ is increased, however, the dynamics exhibits a transition to chaos that is typical for Hamiltonian systems (for an introduction to chaos in Hamiltonian systems, see Ref. 9). Nonlinear resonances form in regions of phase space where the frequency of the driving field is a harmonic of the frequency with which the undriven particle bounces between the walls. The condition for a nonlinear resonance is $\omega_0 = N\pi p$, where N is an integer. These nonlinear resonances grow as ϵ is increased. For sufficiently large ϵ the resonance zones will overlap and create a region of chaotic motion in the phase space.

The transition to chaos can be illustrated using strobe plots of the motion. Strobe plots are created by selecting an initial point for a trajectory in phase space and plotting the location of the trajectory after each cycle of the driving field. If this procedure is repeated for initial conditions throughout the phase space, a plot of the resulting points gives a detailed picture of the system's dynamics. Figure 1 shows strobe plots for the driven infinite square well at four different field strengths. For $\epsilon = 50$ the motion is regular for large values of momentum, as indicated by the continuous lines running from $x = -1$ to $x = 1$. These curves are known as Komolgorov-Arnol'd-Moser (or KAM) tori. The $N = 1$ nonlinear resonance is clearly visible as a series of half-ellipses centered at $p = \omega_0/\pi \approx 25.5$. The $N = 3$ resonance is visible at $p = \omega_0/(3\pi) \approx 8.5$ (to first order, the driving field does not produce resonances with even values of N). Additionally, there is a scatter of points at small values of p indicating that the low-momentum region of the phase space is chaotic. This region of chaos has formed because the nonlinear resonances with $N > 3$ have already overlapped and destroyed each other, producing chaotic motion as a result.

As ϵ is increased the system becomes increasingly chaotic. For $\epsilon = 500$ the $N = 1$ resonance is still intact (although it is distorted and its location has shifted), but it is now an island in a sea of chaos. As ϵ is increased to 3000 we see that the chaotic sea has grown and the resonance island has split, with the two pieces moving to different areas of the phase space. At $\epsilon = 6200$ the chaotic sea has grown still larger and there is no longer any evidence of structure within it. Note that for all field strengths the motion is regular at very high momenta.

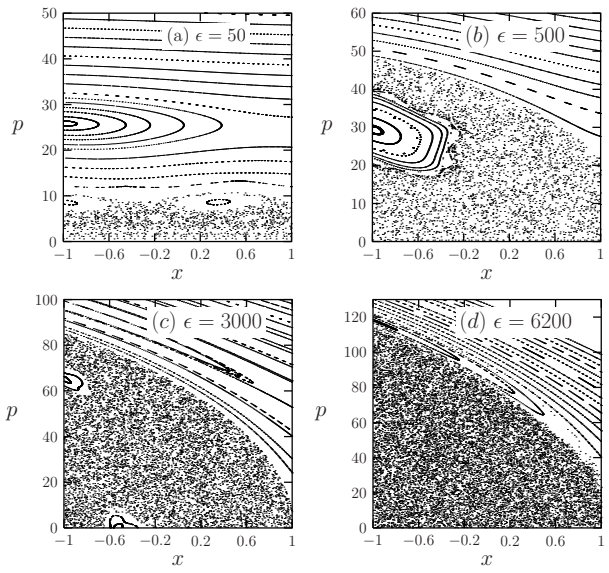

FIG. 1: Strobe plots illustrating the classical dynamics for the driven infinite square well at four different field strengths. Because the system is symmetric in p, only $p \geq 0$ is shown. As the strength of the driving field is increased, nonlinear resonances overlap and produce a large region of chaotic motion at low momenta. At high momenta the motion remains regular.

III. FLOQUET THEORY

As noted above, energy is not a conserved quantity in the driven infinite square well because the Hamiltonian is not symmetric under infinitesimal time translations. Therefore, in analyzing the quantum dynamics of this model we cannot take the usual approach of finding energy eigenvalues and eigenvectors. Recall, though, that this model does possess symmetry under the *discrete* time translation $t \to t + T$. We can take advantage of this symmetry to construct an operator whose eigenvalues and eigenvectors will characterize the dynamics of the system in much the same way that the eigenvalues and eigenvectors of the Hamiltonian characterize the dynamics of energy-conserving systems. The operator that will serve this purpose is the Floquet operator, $\hat{U}(t, t + T)$, which is the unitary time evolution operator that transforms the wavefunction at time t into the wavefunction at time $t + T$:

$$\hat{U}(t, t + T)\psi(t) = \psi(t + T). \tag{3}$$

This operator depends on t, but we can focus our attention on the initial phase of the driving field and calculate the eigenvalues and eigenvectors of the Floquet operator with $t = 0$: $\hat{U}(0, T) = \hat{U}$.

To construct the Floquet operator we will need to solve the time-dependent Schrödinger equation (TDSE). The TDSE for the Hamiltonian of Equation 1 is

$$i\hbar\frac{\partial}{\partial\tilde{t}}|\psi(\tilde{t})\rangle = \left(-\frac{\hbar^2}{2m}\frac{\partial^2}{\partial\tilde{x}^2} + \tilde{\epsilon}\tilde{x}\cos(\tilde{\omega}_0\tilde{t})\right)|\psi(\tilde{t})\rangle, \tag{4}$$

where $|\tilde{x}| \leq a$. We transform to dimensionless coordinates as in the classical system, except that for the quantum system we must scale $\hbar$ rather than $\tilde{p}$: $\hbar = \kappa a\sqrt{2mc}$, where c is the scaled unit of energy and κ now plays the role of the "effective" $\hbar$. The transformed TDSE is then

$$i\kappa\frac{\partial}{\partial t}|\psi(t)\rangle = \left(-\kappa^2\frac{\partial^2}{\partial x^2} + \epsilon x\cos(\omega_0 t)\right)|\psi(t)\rangle, \quad (5)$$

where $|x| \leq 1$. The quantum system has three parameters (ω_0, ϵ, and κ), only two of which are independent. We are not concerned here with the κ-dependence of the dynamics so we will choose $\kappa = 1$ (and $\omega_0 = 80$ as above).

To numerically solve the TDSE we will use a basis consisting of energy eigenstates of the undriven infinite square well. The energy eigenvalues and eigenfunctions for the infinite square well, which are familiar to students of quantum mechanics, are given (in the dimensionless coordinates of our model) by:

$$E_n = \frac{\pi^2\kappa^2 n^2}{4} = \frac{\pi^2 n^2}{4}, \quad (6)$$

$$\langle x|E_n\rangle = \sin\left(\frac{\pi n(x-1)}{2}\right) \quad (7)$$

where n is a positive integer. To determine how many basis states to use in our calculation we can simply look at the classical strobe plots shown in Figure 1. To obtain accurate Floquet eigenstates in the chaotic region we must ensure that our basis extends well into the high-momentum regular region of the phase space. For example, if we examine Figure 1(d) we see that the chaotic region extends to $p = 115$. Recall that for the scaled version of our model (Eq. 2) the kinetic energy of the particle is p^2, so for $\epsilon = 6200$ our basis must extend in energy beyond $115^2 = 13,225$. Setting $E_n = 13,225$ and solving for n we find that our basis must extend beyond $n = 73$ to completely cover the chaotic region of phase space at $\epsilon = 6200$.

In the basis we have chosen the wavefunction of the particle at time t can be written as $|\psi(t)\rangle = \sum_n c_n(t)|E_n\rangle$. The TDSE can then be transformed into a differential equation for the coefficients $c_n(t)$:

$$\frac{dc_n(t)}{dt} = -i\frac{E_n}{\kappa}c_n(t) - \frac{i}{\kappa}\epsilon\cos(\omega_0 t)\sum_m x_{nm}c_m(t), \quad (8)$$

where

$$x_{nm} = \begin{cases} 0, & (m+n) \bmod 2 = 0 \\ \frac{16mn}{\pi^2(m^2-n^2)^2}, & (m+n) \bmod 2 = 1, \end{cases} \quad (9)$$

is the dipole matrix in our basis. To construct the Floquet operator we calculate the coefficients $c_n(T)$ by numerically integrating Eq. 8 with initial condition $c_k(0) = 1$ and $c_n(0) = 0$ for $n \neq k$. The resulting coefficients form the k^{th} column of the Floquet matrix. Once the Floquet matrix is constructed its eigenvalues and eigenvectors can be computed numerically. The Floquet eigenstates are labeled by numbering them in order of increasing expectation value for the undriven Hamiltonian: $H_\alpha = \langle q_\alpha|p^2|q_\alpha\rangle$. The eigenvalues of the Floquet operator must be of the form $\exp(-i\theta)$ because the Floquet operator is unitary and must have eigenvalues of unit modulus. The eigenvalues and eigenvectors of the Floquet matrix satisfy

$$\hat{U}|q_\alpha\rangle = e^{-iq_\alpha T/\kappa}|q_\alpha\rangle, \quad (10)$$

where q_α is called the *quasienergy* of the state $|q_\alpha\rangle$. Because $\exp(-i2\pi) = 1$ we see that q_α is only defined modulo ω_0/κ.

IV. EIGENSTATES

In order to compare the quantum dynamics to the classical dynamics we must be able to represent the Floquet eigenstates in phase space. This requires a bit of subtlety. The uncertainty principle prevents us from defining a quantum wavefunction as a function of both x and p, because we can't assign a probability for the particle to have simultaneous values for x and p. Instead we can construct a Husimi distribution[10], which is a smoothed version of the Wigner distribution.[11] The Husimi distribution gives us the probability for a particle to be found in a region of area $\hbar$ centered on a point in phase space. By smoothing the probability distribution for the particle over regions of area $\hbar$ the Husimi distribution avoids conflicting with the uncertainty principle but still provides a general picture of where in phase space the particle is likely to be found.

To construct the Husimi distribution of a quantum state we calculate the overlap between the quantum state and a minimum uncertainty wavepacket centered on the point (x_0, p_0) in phase space. The wavefunction for this wavepacket is

$$\langle x|x_0, p_0\rangle = \frac{\exp\left(-\frac{(x-x_0)^2}{2\sigma^2} + \frac{ip_0(x-x_0)}{\kappa}\right)}{(\sigma^2\pi)^{1/4}}, \quad (11)$$

where the width of the wavepacket in the x-direction is $\Delta x = \sigma/\sqrt{2}$ and the width in the p-direction is $\Delta p = \kappa/(\sigma\sqrt{2})$. We use $\sigma = 0.158$ in the dimensionless units of our model (σ has the same units as x). The Husimi distribution of the state $|q_\alpha\rangle$ is constructed by calculating the quantity $h_\alpha(x_0, p_0) = |\langle x_0, p_0|q_\alpha\rangle|^2$ on a grid of points in phase space. A contour plot of $h_\alpha(x_0, p_0)$ provides a visual picture of how the quantum state $|q_\alpha\rangle$ is distributed in phase space.

Husimi distributions of several Floquet eigenstates for $\epsilon = 500$ are shown in Figure 2. Comparing these Husimi distributions to the strobe plot in Fig. 1(b) shows a close correspondence between the structure of the quantum eigenstates the structure of the classical phase space. State 29 (Fig. 2(a)) lies along the KAM tori in the high energy region of the classical phase space. State 24 (Fig. 2(b)) lies in the center of the $N = 1$ nonlinear resonance of the classical phase space. State 8 (Fig. 2(c))

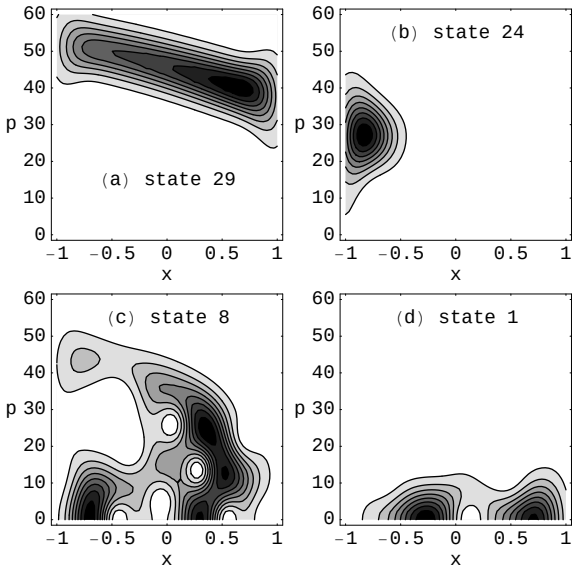

FIG. 2: Husimi distributions of four Floquet eigenstates for $\epsilon = 500$. Note how the distributions shown in (a)-(c) correspond to the different regions of the classical phase space in Fig. 1(b). The distribution shown in (d) is peaked on a line of marginally stable periodic orbits that lie along $p = 0$.

is spread throughout the classically chaotic region. Note, however, that this Floquet state is not spread uniformly but has well-defined peaks and valleys. Quantum eigenstates that lie in classically chaotic regions often show enhanced probability at the locations of unstable periodic orbits of the classical dynamics. States with this property are called *scars*[12] and have been found in a wide variety of quantum systems. State 1 (Fig. 2(d)) also is in the chaotic region of the classical phase space, but it is confined to the region near $p = 0$. Even this state is displaying a quantum-classical correspondence because it is peaked on a continuous line of marginally stable perioidic orbits that lie along $p = 0$ in the classical phase space.[13]

Examples of "chaotic" Floquet states at $\epsilon = 3000$ and $\epsilon = 6200$ are shown in Figure 3. Comparing these Husimi distributions to the classical strobe plots of Fig. 1 we see that these Floquet states are spread throughout the classically chaotic region in each case. As the chaotic region grows, the Floquet states in that region grow with it. In addition, more Floquet states will occupy the chaotic region since the number of quantum states occupying a given region of phase space is proportional to the area of that region. Note, however, that the Floquet states at very high momenta will retain their regular character in correspondence with the classical dynamics.

V. EIGENVALUES

It is perhaps not too surprising that the structure of quantum eigenstates would mimic the structure of classical phase space. However, it may come as a surprise that some properties of the quantum *eigenvalues* of a system are closely tied to the classical dynamics. In fact, in systems whose classical dynamics is completely chaotic it can be shown that the entire set of (quasi)energy eigenvalues is determined by the unstable periodic orbits of the classical motion.[3] In our model the phase space is always a mixture of regular and chaotic motion, and in this case the exact connection between the quantum eigenvalues and the classical dynamics is less clear. However, it can be shown that certain statistical properties of the quantum eigenvalues depend on whether the corresponding classical system is chaotic or regular (see, for example, Reference 15).

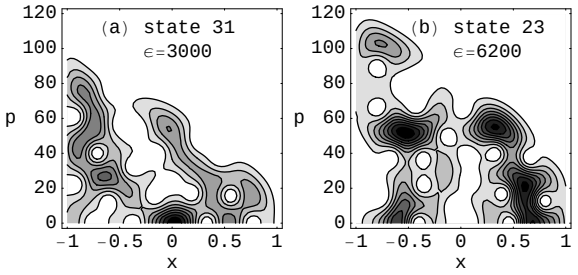

FIG. 3: Husimi distributions of two "chaotic" Floquet states. Note how the distributions correspond to the chaotic region of the strobe plots in Figures 1(c) and 1(d).

Here we will focus on one particular property of the eigenvalues: the distribution of level spacings. Level spacings are the differences between adjacent eigenvalues. The level spacing density, $P(s)ds$, is defined to be the probability that the spacing, s, between any two neighboring eigenvalues lies in the interval $s \to s + ds$.[1] We will assume in the following that the spacings have been scaled so that the average spacing is one. For systems with regular classical dynamics the quantum eigenvalues are random and the level spacings are expected to follow a Poisson distribution

$$P(s) = e^{-s}. \tag{12}$$

For systems with chaotic classical dynamics the quantum eigenvalues are known to have the same statistical properties as the eigenvalues of random matrices. Using ensembles of random 2×2 Hermitian matrices Wigner derived[16] what is known as the Gaussian Orthogonal Ensemble (GOE) distribution[17]

$$P(s) = \frac{\pi s}{2} e^{-\pi s^2/4}. \tag{13}$$

Since we are looking at quasienergies (which are derived from the eigenvalues of the unitary Floquet matrix) rather than energy eigenvalues, we must instead consider the distribution of level spacings for random unitary matrices (known as the Circular Orthogonal Ensemble, or COE). For large matrices the level spacing distribution for the COE is identical to the GOE distribution given

above.[18] In the driven infinite square well we expect to see a change from Poisson statistics to COE statistics, at least among the states that lie in the low momentum chaotic region, as ϵ is increased.

Calculating a numerical spacing distribution would seem to be straightforward for our model. Once we have numerically determined the quasienergies at a given field strength we can simply find the differences between consecutive quasienergies. These spacings can then be grouped into bins and displayed on a histogram that can be compared to the theoretical distributions given above. However, there are a few issues we must consider. First, we must have a sufficiently large number of spacings if we want to make comparisons between the histogram of our data and the theoretical distributions. The second consideration is much more subtle. Recall from Section II that the Hamiltonian of our model is invariant under the generalized parity transformation $x \to -x$ and $t \to t+T/2$. The probability distributions for the Floquet eigenstates must also be invariant under this transformation. Therefore, the Floquet eigenstates can be grouped into two classes: even states whose wavefunctions are unchanged by the generalized parity transformation and odd states whose wavefunctions change sign under the generalized parity transformation. We expect the level spacings for each class of Floquet states to change from Poisson to COE as ϵ is increased. A combination of two Poisson data sets will still follow Poisson statistics (because if you combine two sets of random numbers you get a set of random numbers). If we combine two sets of COE data, though, the combination will not follow the COE statistics. Instead we expect a combination of two COE data sets to produce a level spacing distribution given by[15]

$$P(s) = \frac{1}{2}e^{-\pi s^2/8} + \frac{\pi s}{8}e^{-\pi s^2/16}\mathrm{erfc}\left(\frac{\sqrt{\pi}s}{4}\right), \qquad (14)$$

where $\mathrm{erfc}(z) = (2/\sqrt{\pi})\int_z^\infty dt\exp(-t^2)$ is the complementary error function.

Figure 4 shows a comparison between our numerical data and the theoretical predictions at several field strengths. Each plot shows a histogram of our numerical data as well as the theoretical curves for the Poisson distribution (Eq. 12) and the distribution for 2 sets of COE data (Eq. 14). The data for $\epsilon = 0$ (Figure 4(a)) was generated by calculating the first twenty thousand values of E_n (modulo 80) because for $\epsilon = 0$ the quasienergies are just the energy eigenvalues (modulo ω_0/κ) of the undriven infinite square well. The histogram for $\epsilon = 0$ matches the Poisson curve almost exactly. The data shown in Figures 4(b)-(d) were generated with the numerical procedure described in Section III. Only the states with the 40 lowest values of H_α (which are the states that sit in the low momentum chaotic region for large ϵ) were used in determining the spacings. In each case the histogram shows a combination of spacing data for several field strengths. For example, the data in Figure 4(b) combines spacing data for ϵ = 400, 500, 600, 700, 800, and 900. In each case there were a total of 240 quasienergies used in determining the histogram of level spacings. There is a clear change in the level spacing statistics as ϵ is increased. The histograms in Figures 4(b) and 4(d) are much closer to the distribution for 2 COEs.

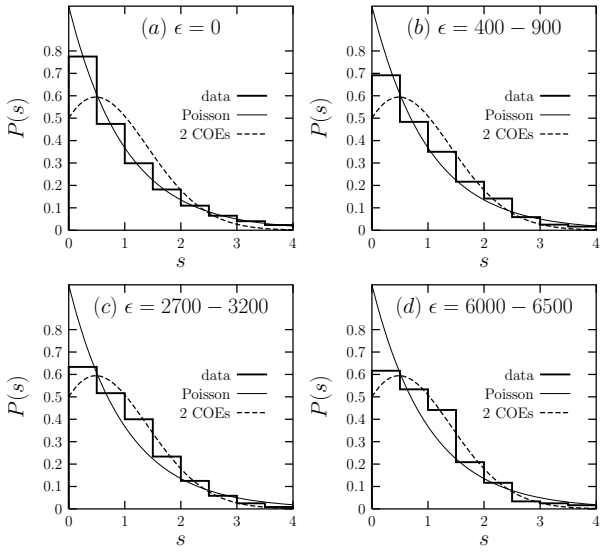

FIG. 4: A comparison of numerically calculated level spacing distributions (histogram) to the distributions for Poisson statistics (thin line) and for a combination of two data sets following COE statistics (dashed line). The spacings have been scaled so that the mean spacing $\langle s\rangle = 1$. The histogram in (a) represents data for 20,000 eigenvalues at $\epsilon = 0$. The histogram in (b) represents data for the 40 states with the lowest values of H_α at six different field strengths ranging from 400 to 900. The remaining histograms are similar to (b) but with ϵ ranging (c) from 2700 to 3200 and (d) from 6000-6500. Note that the data matches the Poisson curve at $\epsilon = 0$ but switches over to the curve for 2 COEs as ϵ is increased.

With some additional effort it is possible to separate the eigenstates of even and odd generalized parity. Each eigenstate can be examined individually to determine whether it is even or odd under the generalized parity transformation. To do this we integrate the TDSE using the eigenstate to be examined as the initial condition. The integration is carried out from $t = 0$ to $t = T/2$. The eigenstate $\psi_\alpha(x,t)$ is even under the generalized parity transformation if

$$\psi_\alpha(-x, T/2)\exp(iq_\alpha T/(2\kappa)) = \psi_\alpha(x,0)$$

and odd if

$$\psi_\alpha(-x, T/2)\exp(iq_\alpha T/(2\kappa)) = -\psi_\alpha(x,0).$$

Once each eigenstate is examined in this way, the spacings between eigenvalues for eigenstates of the same generalized parity can be found. Once these spacings are calculated for each class, the spacing data can be recombined and binned to form a histogram that can be compared with the theoretical predictions of Eqns. 12 and 13.

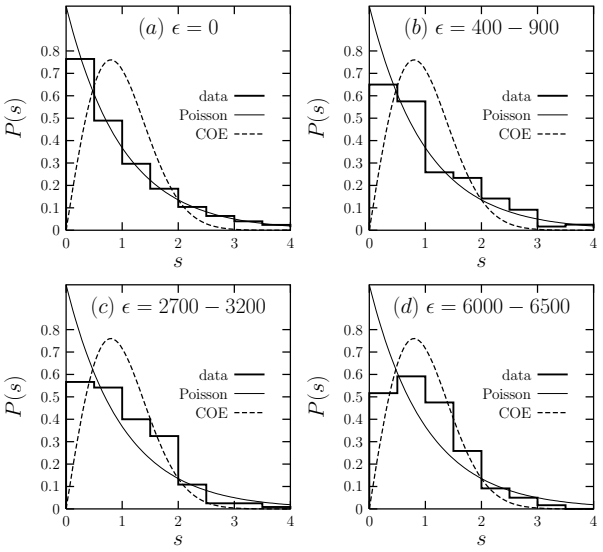

FIG. 5: A comparison of numerically calculated level spacing distributions (histogram) to the distributions for Poisson statistics (thin line) and COE statistics (dashed line). The spacings have been scaled so that the mean spacing $\langle s \rangle = 1$. The histogram in (a) represents data for 20,000 eigenvalues at $\epsilon = 0$, but only spacings between members of the same parity class were used. The histogram in (b) represents data for the 20 states with the lowest values of H_α in each generalized parity class at six different field strengths ranging from 400 to 900. The remaining histograms are similar to (b) but with ϵ ranging (c) from 2700 to 3200 and (d) from 6000-6500. Note that the data matches the Poisson curve at $\epsilon = 0$ but switches over to the COE curve as ϵ is increased.

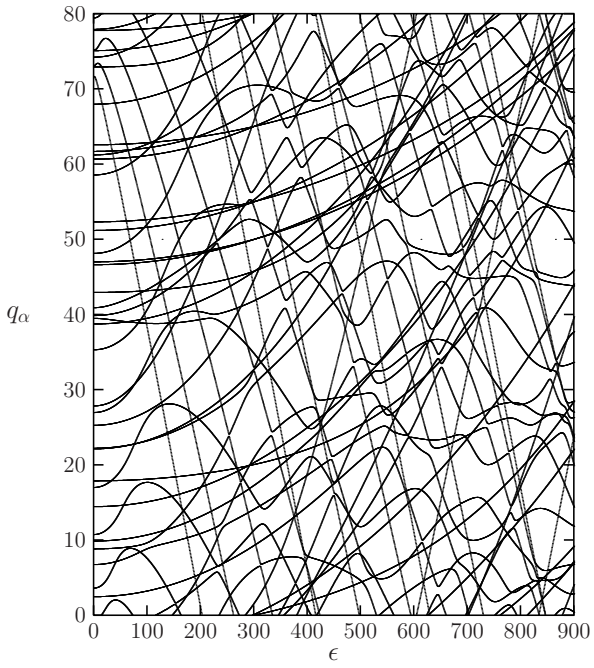

FIG. 6: Quasienergies of the driven infinite square well as a function of ϵ. A basis of 40 eigenstates of the undriven square well was used to calculate these quasienergies. This basis extends well into the regular region of phase space for the field strengths shown. Note the increase in the number of avoided crossings as ϵ is increased.

Figure 5 shows the results of this analysis. The data in Figure 5(a) was generated from the first 20,000 eigenvalues of the undriven infinite square well, but only spacings between states of the same parity class were calculated. The resulting histogram is in excellent agreement with the Poisson distribution of Eq. 12. The data in Figs. 5(b)-(d) was generated using the 20 states with the lowest values of H_α in each generalized parity class. Eigenvalues from six different field strengths were combined in each plot, so each histogram represents 240 quasienergies. The distribution of quasienergy spacings shows a clear transition from Poisson statistics to COE statistics as the field strength is increased.

The most obvious distinction between Poisson and COE statistics is that the COE distribution predicts far fewer small spacings. The Poisson distribution is peaked at $s = 0$, while the COE distribution goes to zero at $s = 0$. Quantum systems that follow COE statistics are said to exhibit *level repulsion*, because the eigenvalues seem to avoid coming near each other. This phenomenon is clearly illustrated by plotting the quantum eigenvalues as a function of the nonlinearity parameter. Figure 6 shows the quasienergies for the driven square well as function of ϵ. Although the eigenvalue curves frequently cross each other at low ϵ, they tend to avoid crossing at higher values of ϵ. The onset of avoided crossings as ϵ is increased indicates level repulsion and the transition to COE level spacing statistics. Moreover, there is evidence that avoided crossings are associated with changes in the phase space structure of the Floquet states.[19] So avoided crossings are not only a third feature of quantum chaos, but also they provide a link between the other two features we have already discussed.

VI. RADIATION SPECTRA

The features of quantum chaos discussed so far may seem far removed from practical experiments. There are, however, signs of the transition to chaos in our quantum model that could be easily observed in experiments. The radiation spectrum produced by a quantum particle in the driven infinite square well can display a phenomenon called high-harmonic generation (HHG) that is closely tied to chaos in the classical version of the system. In HHG the radiation spectrum shows harmonic peaks of roughly constant intensity out to some large harmonic of the driving field.[5] Beyond this "cutoff" the spectrum falls off exponentially.

To calculate the radiation spectrum for a single Floquet eigenstate we must solve the TDSE over several cycles of the driving field using the Floquet eigenstate as our initial condition. Integrating over more cycles produces a higher resolution spectrum. Once the TDSE has

been solved we calculate an acceleration time series given by

$$\langle\psi(t)|\ddot{x}|\psi(t)\rangle = \sum_{m,n} c_n^*(t)\ddot{x}_{nm}c_m(t), \tag{15}$$

where the c's are the coefficients from Equation 8 and

$$\begin{aligned}\ddot{x}_{nm} &= -\frac{1}{\kappa^2}(E_n - E_m)^2 x_{nm} \\ &\quad + \frac{1}{\kappa^2}\epsilon\cos(\omega_0 t)\sum_k (2E_k - E_n - E_m)x_{nk}x_{km}\end{aligned} \tag{16}$$

is the "acceleration matrix element." The power spectrum is then estimated by calculating the square modulus of the Fourier transform $\chi(\omega)$ of the acceleration time series.

Figure 7 shows radiation spectra for several Floquet states. In each case the TDSE was integrated over 16 cycles of the driving field. This is actually unnecessary because the Floquet eigenstate wavefunctions are periodic in time with period T. However, integrating over several cycles provides greater frequency resolution and illustrates the fact that the Floquet eigenstates radiate only at harmonics of the driving field. In fact, Figure 7 shows that the Floquet states radiate only at *odd* harmonics of the driving field. The even harmonics are suppressed because of the spatial symmetry of the infinite square well.

Figure 7(a) shows the spectrum for the state shown in Figure 2(a), which does not exhibit HHG. There is a dramatic falloff in power after the first harmonic. This is characteristic of Floquet states that lie in regular regions of the phase space. By contrast the spectrum in Figure 7(b) shows clear HHG with no dramatic falloff in power until after the 25^{th} harmonic. This state is spread throughout the chaotic region (see Fig. 2(d)) and it's cutoff is determined by the energy range spanned by the chaotic sea. This energy range is given by $p_{\max}^2 - p_{\min}^2$, where $p_{\max}$ and $p_{\min}$ are the maximum and minimum magnitudes of momentum in the chaotic region ($p_{\min} = 0$). Setting this energy range equal to the maximum photon energy we find that the classical prediction for the cutoff is

$$\omega_{\max}/\omega_0 = p_{\max}^2/(\kappa\omega_0). \tag{17}$$

Since the cutoff in Fig. 7(b) occurs at the 25^{th} harmonic this corresponds to $p_{\max} \approx 45$ for $\epsilon = 500$. Note that this value is indeed close to the top of the chaotic sea in Fig. 1(b). Similar results are found for the spectrum in Fig. 7(c) which has a cutoff at the 149^{th} harmonic. This corresponds to $p_{\max} \approx 109$ for $\epsilon = 6200$. This result is in agreement with the strobe plot shown in Fig. 1(d). Thus we see that the structure of the classical phase space helps determine the radiation spectra of Floquet eigenstates. States that are spread throughout a chaotic region of phase space exhibit HHG with a cutoff determined by the energy range of the chaotic sea, while states that lie in regular regions display no HHG and radiate almost exclusively at the first harmonic.

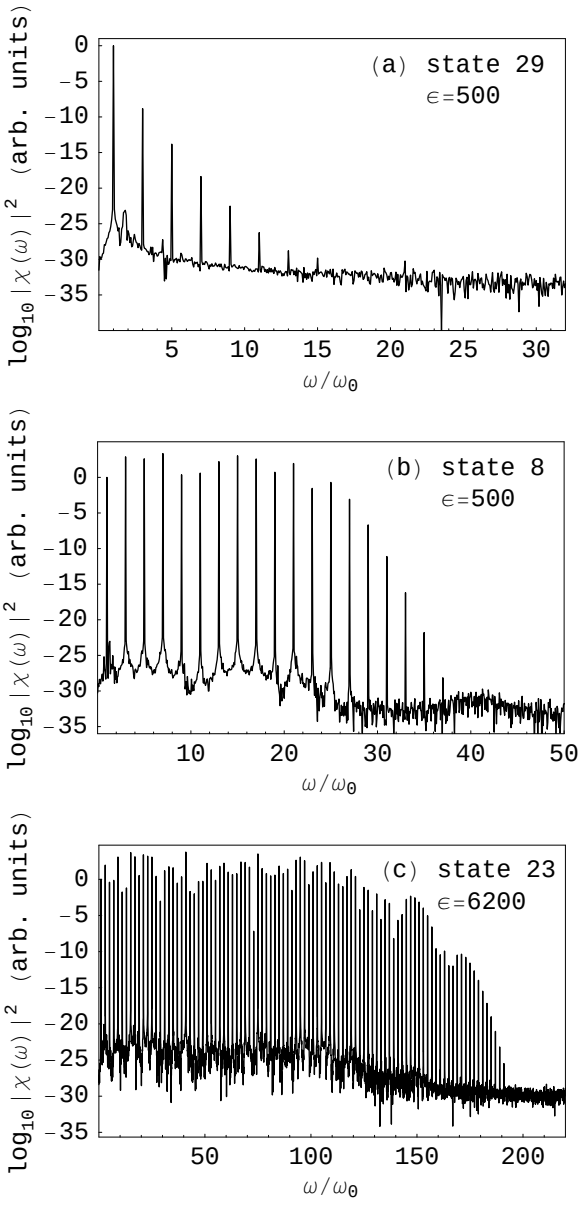

FIG. 7: Radiation spectra for several Floquet states. The spectrum shown in (a) is for state 29 at $\epsilon = 500$ (see Fig. 2(a)) and exhibits no HHG. The spectrum in (b) is for state 8 at $\epsilon = 500$ (see Fig. 2(d)) and exhibits HHG with a cutoff near the 25^{th} harmonic. The spectra in (c) is for state 23 at $\epsilon = 6200$ (see Fig. 3(b)) and has a cutoff near the 149^{th} harmonic.

VII. QUANTUM CHAOS IN THE CLASSROOM

The material presented here could be developed into an enrichment activity for students in an undergraduate (or beginning graduate) course in quantum mechanics. To this end, a Mathematica notebook is provided which can be used to carry out many of the calculations presented in this paper.[21] FORTRAN programs that can be used to carry out any of the calculations presented here are available by request. Armed with these computational tools

students can explore the structure of Floquet eigenstates, level spacing distributions, and radiation spectra for the driven square well at a variety of field strengths. For example, students could calculate the radiation spectra for the states shown in Figs 2(b) and 3(a) to determine how the spectra relate to the structure of the eigenstates and the classical dynamics. One particularly interesting problem would be to investigate what happens to the quantum dynamics when too few basis states are used in the calculation. Students could be asked to investigate the eigenstates, level spacing statistics, and radiation spectra at $\epsilon = 6200$ using only 40 basis states. Since the basis covers only a portion of the chaotic region in the phase space, this will not provide an accurate description of the quantum dynamics of the driven square well system for these parameter values. However, the calculations do pertain to *some* quantum system. By analyzing the quantum dynamics of this system one can determine if the (unknown) corresponding classical system is chaotic.[22]

VIII. SUMMARY AND DISCUSSION

The classical and quantum dynamics of the driven infinite square well was examined as the strength of the driving field is increased. The classical dynamics shows a clear transition from regular to chaotic motion at low momenta, as can be seen by the formation of a large chaotic sea in strobe plots of the classical motion. The quantum dynamics undergoes a number of changes that correspond to this transition to chaos in the classical dynamics. The Floquet eigenstates exhibit phase space structure that mimics the structures seen in the classical phase space. In particular, as the the field strength is increased many of the Floquet eigenstates become spread out over the classically chaotic region of phase space. The quasienergies also exhibit a transition, with the distribution of level spacings changing from a Poisson distribution to a COE distribution as the classical system becomes increasingly chaotic. Both of these changes are connected with avoided crossings in the eigenvalue spectrum. Finally, the cutoff for high harmonic generation in the radiation spectrum of a chaotic Floquet state was shown to be determined by the energy range of the chaotic sea in the classical phase space.

Because the model of the driven infinite square well is relatively simple, this material could be incorporated into an advanced undergraduate or beginning graduate course in quantum mechanics. A Mathematica notebook[21] that implements many of the calculations described here is available for this purpose. Finally, it should be mentioned that this simple system has been used to model real systems like $GaAs/Al_xGa_{1-x}As$ quantum wells subject to intense far-infrared radiation.[23]

Acknowledgments

The author would like to thank Frank Petruzielo for carrying out some of the computations for this work.

* Electronic address: ttimberlake@berry.edu

[1] Linda E. Reichl, *The Transition to Chaos in Conservative Classical Systems: Quantum Manifestations* (Springer-Verlag, New York, 1992).

[2] Fritz Haake, *Quantum Signatures of Chaos* 2nd ed. (Springer-Verlag, Berlin, 2001).

[3] Martin C. Gutzwiller, *Chaos in Classical and Quantum Mechanics* (Springer-Verlag, New York, 1990).

[4] Hans-Jürgen Stöckmann, *Quantum Chaos: An Introduction* (Cambridge University Press, New York, 1999).

[5] Zenghu Chang, Andy Rundquist, Haiwen Wang, Margaret M. Murnane, and Henry C. Kapteyn, "Generation of Coherent Soft X Rays at 2.7 nm Using High Harmonics," Phys. Rev. Lett. **79**, 2967-2970 (1997).

[6] J. E. Bayfield and P. M. Koch, "Multiphoton Ionization of Highly Excited Hydrogen Atoms," Phys. Rev. Lett. **33**, 258-261 (1974).

[7] F. L. Moore, J. C. Robinson, C. Bharucha, P. E. Williams, and M. G. Raizen, "Observation of Dynamical Localization in Atomic Momentum Transfer: A New Testing Ground for Quantum Chaos," Phys. Rev. Lett. **73**, 2974-2977 (1994); Daniel A. Steck, Windell H. Oskay, and Mark G. Raizen, "Observation of Chaos-Assisted Tunneling Between Islands of Stability" Science **293**, 274-278 (2001).

[8] W. A. Lin and L. E. Reichl, "External field induced chaos in an infinite square well potential," Physica **19D**, 145-152 (1986).

[9] Todd Timberlake, "A computational approach to teaching conservative chaos," to be published in Am. J. Phys.

[10] Kin'ya Takahashi, "Distribution Functions in Classical and Quantum Mechanics," Prog. Theor. Phys. Supp. **98**, 109-156 (1989).

[11] M. Belloni, M. A. Doncheski, and R. W. Robinett, "Wigner quasi-probability distribution for the infinite square well: Energy eigenstates and time-dependent wave packets," Am. J. Phys. **72**, 1183-1192 (2004).

[12] Eric J. Heller, "Bound-State Eigenfunctions of Classically Chaotic Hamiltonian Systems: Scars of Periodic Orbits," Phys. Rev. Lett. **53**, 1515-1518 (1984).

[13] Todd Timberlake, Frank Petruzielo, and Linda E. Reichl, unpublished.

[14] N. Moiseyev, H. J. Korsch, and B. Mirbach, "Classical and quantum chaos in molecular rotational excitation by ac electric fields," Z. Phys. D **29**, 125-138 (1994).

[15] David L. Kaufman, Ioan Kosztin, and Klaus Schulten, "Expansion method for stationary states of quantum billiards," Am. J. Phys. **67**, 133-141 (1999).

[16] E. P. Wigner, "Distribution laws for the roots of a random Hermitian matrix," in *Statistical theories of spectra: fluctuations*, ed. C. E. Porter, Academic Press, New York (1965).

[17] One must be careful when determining the level spacing distribution for a chaotic system because different distributions should be used for different classes of Hamiltonian

or Floquet operators. The distribution given in the text is the correct one for this system. A more detailed account of this issue can be found in Haake's text (Ref. 2).

[18] M. L. Mehta, *Random Matrices and the Statistical Theory of Energy Levels* 2nd ed. (Academic Press, New York, 1991).

[19] T. Timberlake and L. E. Reichl, "Changes in Floquet-state structure at avoided crossings: Delocalization and harmonic generation," Phys. Rev. A **59**, 2886-2893 (1999).

[20] Vitali Averbukh and Nimrod Moiseyev, "Cutoff in molecular harmonic-generation spectra resulting from classical chaotic dynamics," Phys. Rev. A **51**, 3911-3915 (1995); W. Chism, T. Timberlake, and L. E. Reichl, "High harmonic generation in systems with bounded chaos," Phys. Rev. E **58**, 1713-1723 (1998).

[21] A Mathematica notebook implementing many of the calculations discussed here can be found at fsweb.berry.edu/academic/mans/ttimberlake/QuantChaos/. FORTRAN programs for carrying out these computations are also available from the author.

[22] It is much more challenging to try to determine the Hamiltonian of the chaotic classical system that corresponds to the quantum system. It is interesting to note that the zeros of the Riemann zeta function have the same statistical properties as eigenvalues of a "chaotic" quantum system, and thus in principal they can be thought of as eigenvalues of *some* quantum system. If you could determine the Hamiltonian of the (chaotic) system that has these eigenvalues you could solve one of the greatest unsolved problems in mathematics!

[23] Björn Birnir, Bryan Galdrikian, Rainer Grauer, and Mark Sherwin, "Nonperturbative resonances in periodically driven quantum wells," Phys. Rev. B **47**, 6795-6798 (1993).